Combined Grid and Feature-based Mapping of Metal Structures with Ultrasonic Guided Waves

Othmane-Latif Ouabi, Pascal Pomarede, Neil Zeghidour, Matthieu Geist, Ayoub Ridani, Nico F Declercq, Cédric Pradalier

Combined Grid and Feature-based Mapping of Metal Structures with Ultrasonic Guided Waves

Othmane-Latif Ouabi[1], Pascal Pomarede[1], Neil Zeghidour[2], Matthieu Geist[2],
Ayoub Ridani[3], Nico F. Declercq[1,3], Cédric Pradalier[1]

Abstract— The ultrasonic mapping of plate-based facilities is an essential step towards the robotic inspection of large metal structures such as storage tanks or ship hulls. This work proposes a novel framework that exploits ultrasonic echoes to recover grid-based and feature-based spatial representations jointly. We aim to improve on a previous mapping method [1] subject to errors due to interference, and which provides plate geometry estimates without uncertainty assessment. The grid can represent, all along the mapping process, both areas identified as inside or outside the current plate and areas whose state is still unknown, making it is suitable *e.g.* for detecting a change of plate, or for use in a later active-sensing strategy. We also leverage the resulting spatial information to filter out candidate plate edges that are no longer relevant, mitigating the detrimental effect of interference. We test the approach in simulation, with acoustic data acquired manually and with a real robot. Results show that it is effective for building combined map representations and robust to echo misdetection, contrary to a more standard mapping approach.

I. INTRODUCTION

This work[4] presents a novel approach for mapping the geometry of structures made of metal panels assembled out together with Ultrasonic Guided Waves (UGWs) to enable long-range acoustic inspection with robotic systems. Such an application holds tremendous potential for industrial purposes, such as the autonomous inspection of ship hulls and storage tanks [2]. Indeed, mapping the edges of the individual metal plates helps recover structure-bound landmarks that can be subsequently used, in combination with external measurements (*e.g.*, accelerometers, ultra-wideband beacons, or laser theodolite, among others), for robot localization within a Simultaneous Localization and Mapping (SLAM) framework. Furthermore, it is an essential step towards the mapping of other acoustic scatterers, such as defects.

UGWs can be generated in metal plates by applying piezoelectric transducers in contact with the surface. These waves propagate radially around the emitter in a direction parallel to the surface, and over long distances. When encountering the plate edges, they are reflected orthogonally, and a receiver can collect the ultrasonic echoes. Thus, the

resulting acoustic data carry essential information on the source position and the plate geometry. Yet, relying on such measurements for ultrasonic mapping is challenging due to the dispersive nature of the waves, which causes wavepacket deformation when the propagation distance increases [3], [4], and due to the presence of multiple overlapping wavepackets in the measurements.

In this work, we establish, through a thorough modeling of measurement errors and echo association, a robust approach based on the Bayesian Occupancy Grid (OG) framework [5] and beamforming [6] for simultaneously recovering a feature-based representation of the geometry of a single plate along with a grid-based representation, given robot poses. The grid can depict areas identified as either inside or outside the current plate and areas whose state is still unknown all along the mapping process. Hence, such a grid helps detect plate boundary-crossing on a large structure and path planning for optimal information retrieval. In our framework, the inverse sensor model of the Bayesian filter is updated online from the feature-based representation. We also derive binary masks from the available spatial information to filter out candidate plate edges that are no longer relevant to mitigate the ambiguity of the geometry determination caused by interference. The results obtained in simulation, with experimental measurements acquired by hand, and with a real inspection robot demonstrate our approach's effectiveness and robustness.

II. RELATED WORK

Inspecting large metal structures usually consist in deploying a mobile robot to perform point-by-point thickness measurements with an acoustic probe [7]. However, the entire surface cannot be inspected in a reasonable amount of time due to the limited surface of the transducer. Alternatively, UGWs can be deployed on static networks of sensors for long-range defect detection and localization [8], [9], [10], or for mapping various structural features such as stiffeners [11], [12]. Nevertheless, they can only be used to inspect local areas. Overall, UGWs have not been deployed on a mobile unit to the best of the authors' knowledge.

Recently, the potential of UGWs for robotic-oriented applications has been demonstrated. In [13], the positions of a co-located emitter/receiver pair of piezoelectric transducers are recovered with a centimeter precision by relying on ultrasonic reflections on metal plate boundaries. In [1], [14], the sensor positions are estimated along with a feature-based plate geometry within a FastSLAM [15] framework. In

[1]Othmane-Latif Ouabi, Pascal Pomarede, Nico F. Declercq and Cédric Pradalier are with GeorgiaTech Lorraine and the IRL2958 GT-CNRS in Metz, France. `firstname.lastname@georgiatech-metz.fr`

[2]Neil Zeghidour and Matthieu Geist are with Google Research, Brain Team. {`neilz, mfgeist`}`@google.com`

[3]Ayoub Ridani and Nico F. Declercq are with Georgia Institute of Technology, Atlanta, GA 30332-0250, USA. {`aridani, declercq`}`@gatech.edu`

particular, centimeter precision on the localization and mapping results is achieved in [1] by relying on beamforming. However, the mentioned approach does not tackle the detrimental effect of interference (see next section), whereas it is a well-known issue of basic beamformers. Furthermore, due to the lack of uncertainty assessment and the time-inconsistent map estimates provided in the early steps, the approach is not suitable for mapping several metal plates on a large structure, which necessitates robust detection of plate boundary-crossing. Indeed, detection failures may result in mapping inaccuracies, as one acoustic measurement contains only information on the current plate. Overall, the method is unsuitable for active sensing, whereas it is shown that the robot trajectory significantly affects the estimation results [1].

Grid-based representations are useful for robotic applications, in particular for exploration [5], [16], [17], as they can explicitly account for explored and unexplored areas. Guided wave-based exploration on a metal plate has been investigated in [18] to autonomously map the inside of a metal panel by relying on such grid representations. However, the multiple echoes within the signals are not exploited in the mapping procedure, and the presence of echo measurement errors is not considered.

Several works have demonstrated the benefit of combining grid and feature-based maps in the robotics literature [19], [20], [21], and are found to surpass classical and single representation-based approaches. This work establishes a methodology to jointly recover a grid and a feature-based representation of metal plates from UGWs measurements. It is shown that such a strategy can mitigate the detrimental effect of interference and overcomes the problems of echo detection errors and echo labelling even in the presence of multiple order reflections. At the same time, such issues are often overlooked in recent works addressing the similar problem of room shape reconstruction from acoustic echoes in the air [22], [23]. Our approach is tested with measurements acquired both by hand and with a magnetic crawler. To the best of the authors' knowledge, this attempt is among the first to successfully demonstrate the practical use of UGWs for mapping plate-like structures with a real robotic platform.

III. METHOD

Our approach builds on feature-based maps estimated via beamforming to construct inverse sensor models in an online fashion, so that a grid representation of the plate can be recovered within the OG framework. Simultaneously, the beamforming maps are filtered with binary masks to mitigate the detrimental effect of interference.

A. Feature-based ultrasonic mapping via beamforming

We consider a mobile unit equipped with co-located piezoelectric transducers for signal emission and reception and moving on a metal surface. During the measurement step i at position x_i, y_i, guided waves are excited in the plate material. The receiver collects the acoustic response, which contains the reflections of the incident wave on the plate boundaries. When a set of measurements have
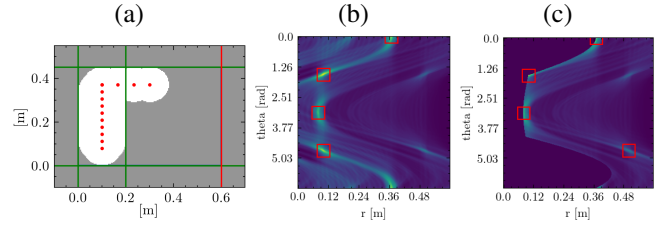

Fig. 1: Filtering beamforming maps with the first acoustic echo for interference rejection. (a) depicts the acquisition positions (red dots) used in the simulated scenario, along with the plate geometry estimate (green lines) recovered from the standard beamforming map shown in (b). The single edge that differs when the geometry is recovered from the filtered beamforming map shown in (c) is the red line in (a). Also, the area identified as "on the plate" with the ground-truth first echo is represented by the lighter area in (a). The line estimates overlay the true outline of the plate.

been acquired along a trajectory $\{x_i, y_i\}_{i=1..t}$, Delay-and-Sum (DAS) beamforming is applied to recover a plate geometry from signals z_i obtained through correlation of the measurements with a wave propagation model [1]. This yields beamforming maps that are computed with:

$$\mathcal{L}_t(r, \theta) = \sum_{i=1}^{t} z_i(d_i(r, \theta)) \triangleq \sum_{i=1}^{t} z_i(|x_i \cdot \cos\theta + y_i \cdot \sin\theta - r|)$$
(1)

where (r, θ) represent the polar coordinates of the line with equation: $x \cdot \cos\theta + y \cdot \sin\theta - r = 0$, while $\mathcal{L}_t(r, \theta)$ indicates the likelihood of the line existence. Next, a feature-based estimate of the map $\hat{M}_t = \{r_l, \theta_l\}_{l=1..4}$ is recovered by extracting the local maxima of $\mathcal{L}_t$ [1] based on the constraint of a rectangular shape (which is *not* a limitation for mapping ship hulls and storage tanks, as they are almost entirely made out of rectangular panels). However, the geometry retrieval may often be ambiguous due to interference, as an infinity of lines can equally account for one range measurement. The effect of interference is further exacerbated by the presence of multiple echoes and high-order reflections that are not considered in Eq. (1). Fig.1-(a) illustrates the interference effect in a simulated scenario, where a mobile unit is driven to acquire acoustic measurements at predetermined positions marked as red points. As most of the measurements are acquired on a line parallel to an edge, there is an ambiguity on which side the real edge is. This results in the boundary on the right not being correctly identified from the beamforming map shown in Fig.1-(b).

The intuition behind the developed approach is that, when relying on detecting the earliest echo within the measurements, which indicates the distance to the closest edge, some information on the spatial environment can be directly integrated into the mapping results. First, it can be inferred that the disk centered at the sensor position whose radius equals the detected range contains only points on the current plate. Second, the lines that cross the total area identified as "on the plate" can be filtered out on the beamforming map to mitigate interference. This principle is illustrated in Fig. 1-

(a)-(c), where all the edges are now correctly identified after applying the mask filter to the beamforming map. The main issue of this approach is that the actual lines may be filtered as well when the measured ranges are overestimated.

B. Grid representation and binary filtering

To obtain a more informative and time-consistent representation of the environment, our approach is designed to recover a grid representation of the 2D space,

$$
O(\mathbf{x}) = \begin{cases} 0 \text{ if } \mathbf{x} = [x, y] \text{ is a point of the plate} \\ 1 \text{ otherwise} \end{cases} \; ,
$$

by constructing an estimate $\hat{O}_t$ with posteriors $\hat{O}_t(\mathbf{x}) = p(O(\mathbf{x}) = 1|\mathbf{x}_{1..t}, z_{1..t})$ based on the detection of the closest edge. However, as the single-use of the detected range cannot be sufficient to recover areas outside the plate, the probability model shall rely on the feature-based map determined via beamforming to estimate the direction of arrival (DoA) of the detected echo. Besides, the introduced representation can be leveraged to filter out lines on $\mathcal{L}_t(r, \theta)$ that are no longer relevant because they cross the area identified as on the plate with $\hat{O}_t$ to mitigate interference. Hence, we formally introduce the mask associated with the ground-truth grid $O(\mathbf{x})$,

$$
Q(r, \theta) = \begin{cases} 0 \text{ if } \exists \mathbf{x} \text{ of the line } (r, \theta) \text{ s.t. } O(\mathbf{x}) = 0 \\ 1 \text{ otherwise} \end{cases} \; ,
$$
(2)

so that the feature-based map $\hat{\mathbf{M}}_t$ can be retrieved from the masked beamforming map, where the mask is to be estimated as well: $\hat{\mathcal{L}}_t(r, \theta) = \hat{Q}_t(r, \theta)\mathcal{L}_t(r, \theta)$. It is critical to rely on a probabilistic approach to avoid erroneously filtering lines. In practice, echo mis-detection may occur due to noise and the propagation model's inaccuracy.

C. Binary filtering with adaptive inverse sensor models

The standard Occupancy Grid (OG) framework is convenient for estimating grids of binary values. It relies on the essential assumptions that the measurements are conditionally independent given the grid state and that the states of the individual grid cells are conditionally independent given a measurement [24]. These assumptions, which are not always realistic, yield a computationally efficient algorithm that can run in real-time. Here, the filter involves an inverse measurement model that will be estimated from all past acoustic data based on the feature-based map retrieved via beamforming: $p(O(\mathbf{x})|\mathbf{x}_t, z_t, \hat{\mathbf{M}}_t)$. More specifically, as $\hat{\mathbf{M}}_t$, which represents the parameters of the inverse model, is updated online, the interpretation of a measurement z_t can vary as well based on DoA estimates. In contrast, the standard OG framework would only involve $p(O(\mathbf{x})|\mathbf{x}_t, z_t)$. Eventually, the grid can be recursively estimated with the standard Bayesian binary filter with log-odds ratios [5] $l_t = \log \frac{\hat{O}_t(\mathbf{x})}{1-\hat{O}_t(\mathbf{x})}$ (and the assumption of a uniform prior):

$$
l_t = l_{t-1} + \log \frac{p(O(\mathbf{x})|\mathbf{x}_t, z_t, \hat{\mathbf{M}}_t)}{1 - p(O(\mathbf{x})|\mathbf{x}_t, z_t, \hat{\mathbf{M}}_t)}
$$

with initial cell values $\forall \mathbf{x}, \hat{O}_0(\mathbf{x}) = 1/2$. For computational efficiency, the same approach is used to build $\hat{Q}_t$ with a second inverse model $p(\hat{Q}_t(r, \theta)|\mathbf{x}_t, z_t, \hat{\mathbf{M}}_t)$. Overall, the major challenge is specifying the two inverse models to determine the mapping strategy fully. In addition, this strategy shall be designed to maintain sufficient consistency between the grid $\hat{O}_t$ and the mask $\hat{Q}_t$, as $\hat{Q}_t(r, \theta)$ should formally depend on the full grid $\hat{O}_t$ as in Eq. (2). However, in our approach, it is computed independently of the later given measurements and beamforming results.

D. Inverse model estimation in the Cartesian space

We first start the construction of a mixture model $p(O(\mathbf{x})|\mathbf{x}_t, z_t, \hat{\mathbf{M}}_t)$ through the modeling of imperfect echo measurements. Let ρ_t be the range to the closest edge detected from z_t. We assume that the echo detection can completely fail with a probability α to construct a model robust to measurement error. In that event, the cell distribution shall be updated with a uniform distribution. With a probability $1-\alpha$, the range is detected with a precision consistent with the wavelength. This is accounted for by introducing the model $p(s|z_t)$ that we model with a truncated Gaussian distribution $p(s|z_t) = \mathcal{N}_{[0,d_{\max}]}(s|\rho_t, \sigma^2)$ of support $[0, d_{\max}]$,

$$
p(s|z_t) = \begin{cases} \frac{1}{\eta\sqrt{2\pi\sigma^2}} \exp\left\{ -\frac{(s-\rho_t)^2}{2\sigma^2} \right\}, \text{if } s \in [0, d_{\max}] \\ 0 \text{ otherwise} \end{cases} \; ,
$$

where η is the normalizing factor and $d_{\max}$ is the maximum detectable range that is introduced due to the finite observation window of the signals. The variable s denotes possible values for the range. Hence, the inverse model can first be expressed as a mixture and using a convolution:

$$
p(O(\mathbf{x})|\mathbf{x}_t, z_t, \hat{\mathbf{M}}_t) = \frac{\alpha}{2}
$$
$$
+ (1 - \alpha) \int p(O(\mathbf{x})|\mathbf{x}_t, \hat{\mathbf{M}}_t, s)p(s|z_t)\, ds. \quad (3)
$$

To build the model $p(O(\mathbf{x})|\mathbf{x}_t, \hat{\mathbf{M}}_t, s)$ which would state how the probability is updated for a given detected range s, we consider two scenarios. In the first one, the DoAs provided by $\hat{\mathbf{M}}_t$ would not be taken into account because the detected range would not be consistent with the expected range: *i.e* the map $\hat{\mathbf{M}}_t$ is assumed to be erroneous as it does not contain any line that is consistent with the range measurement, given that echo misdetection is already modeled with the probability α. To account for this scenario, we introduce a model: $p_1(O(\mathbf{x})|\mathbf{x}_t, s) = H(|\mathbf{x}_t - \mathbf{x}| - s)/2$ where H denotes the Heaviside's function, $H = \mathbf{1}_{s>0}$. Hence, only the points closer than the presumed range s can be marked as "on the plate", while those further away would have unchanged distribution. Let us first assume that $p(O(\mathbf{x})|\mathbf{x}_t, \hat{\mathbf{M}}_t, s)$ is represented only by this model. As it is convolved in Eq. (3) with the truncated Gaussian distribution, the distribution updates are weighted with the range likelihoods. The convolution can seamlessly be expressed with the error function:

$$\int H(|\mathbf{x}_t - \mathbf{x}| - s)\mathcal{N}_{[0,d_{\max}]}(s|\rho_t, \sigma^2)ds$$

$$= \frac{\Phi_t(|\mathbf{x}_t - \mathbf{x}|) - \Phi_t(0)}{\Phi_t(d_{\max}) - \Phi_t(0)}; \Phi_t(z) = \operatorname{erf}\left(\frac{z - \rho_t}{\sigma\sqrt{2}}\right).$$

Nevertheless, only points that are believed to be on the current plate are being recovered with the current model, and there is no mechanism for estimating areas outside the plate. To remedy that, we introduce a second model that will be used to integrate the information from $\hat{\mathbf{M}}_t$. Let's consider that the retrieval of a range s might originate from a reflection of the incident wave on an edge with polar coordinates $(\hat{r}, \hat{\theta})$ from $\hat{\mathbf{M}}_t$. We introduce a second model to update the cells in the specific direction $\hat{\theta}$ and beyond the range s,

$$p_2(O(\mathbf{x})|\mathbf{x}_t, (\hat{r}, \hat{\theta}), s) = \frac{1}{2}\beta(\hat{r}, \hat{\theta}, s, \mathbf{x}_t)\times$$

$$H\left((x - x_t)\cos\hat{\theta} + (y - y_t)\sin\hat{\theta} - s\right),$$

so that the cell occupancy probability can also increase. As the range-line association is not necessarily correct, we have introduced an association coefficient β between 0 and 1 that will make the probability update effective only when the considered range s matches with that expected from a reflection on the edge $(\hat{r}, \hat{\theta})$, and with Gaussian distribution to model uncertainty on the line parameters: $\beta(\hat{r}, \hat{\theta}, s, \mathbf{x}_t) = \exp\{-\frac{1}{2b^2}(|x_t \cdot \cos\hat{\theta} + y_t \cdot \sin\hat{\theta} - \hat{r}| - s)^2\}$. For simplicity, the two aforementioned sub-models are then assembled together through averaging, yielding for a single line of the feature-based map: $p(O(\mathbf{x})|\mathbf{x}_t, (\hat{r}, \hat{\theta}), s) = \frac{1}{2}(p_1(O(\mathbf{x})|\mathbf{x}_t, s) + p_2(O(\mathbf{x})|\mathbf{x}_t, (\hat{r}, \hat{\theta}), s))$. This will result in Eq. (3) in the convolution of the model p_2 with the truncated Gaussian which can also be expressed with the error function:

$$\int \beta(\hat{r}, \hat{\theta}, s, \mathbf{x}_t)H\left((x - x_t)\cos\hat{\theta} + (y - y_t)\sin\hat{\theta} - s\right)\times$$

$$\mathcal{N}_{[0,d_{\max}]}(s|\rho_t, \sigma^2)ds$$

$$= \frac{\Gamma_{t,\hat{r},\hat{\theta}}\left((x - x_t)\cos\hat{\theta} + (y - y_t)\sin\hat{\theta}\right) - \Gamma_{t,\hat{r},\hat{\theta}}(0)}{\Phi(d_{\max}) - \Phi(0)}$$

where $\Gamma_{t,\hat{r},\hat{\theta}}(z) = \frac{\lambda_t(\hat{r},\hat{\theta})\cdot\sigma_{\text{new}}}{\sigma}\operatorname{erf}\left(\frac{z - \mu_{\text{new}}}{\sigma_{\text{new}}\sqrt{2}}\right)$, $\mu_{\text{new}} = \frac{b^2\rho_t + \sigma^2 d_t(\hat{r},\hat{\theta})}{b^2 + \sigma^2}$, $\sigma_{\text{new}} = \frac{\sigma b}{\sqrt{b^2 + \sigma^2}}$ and $\lambda_t(\hat{r}, \hat{\theta}) = \exp(-\frac{(\mu_{\text{new}} - \rho_t)^2}{2\sigma^2} - \frac{(\mu_{\text{new}} - d_t(\hat{r},\hat{\theta}))^2}{2b^2})$. Yet, we have so far considered that only one line is available, whereas the full feature-based map $\hat{\mathbf{M}}_t$ possesses four lines. Hence, for updating the state of the cell $\hat{O}_t(\mathbf{x})$, we take the maximum value of the convolution terms over the lines, so that the probability that $\mathbf{x}$ is outside the plate can be increased as soon as there is at least one line estimate that is consistent with the range measurement. Furthermore, we introduce a coefficient $\mathcal{C}(\mathbf{x}, \mathbf{x}_t, \hat{r}_l, \hat{\theta}_l) = \exp\{-\gamma|(y - y_t)\cdot\cos(\hat{\theta}_l) - (x - x_t)\cdot\sin(\hat{\theta}_l) - \hat{r}_l|\}$ so that the update can be made effective locally around the axis passing through $\mathbf{x}$ and its projection on the line $(\hat{r}_l, \hat{\theta}_l)$. All brought together, the full inverse model in the Cartesian space can be expressed with

$$p(O(\mathbf{x})|\mathbf{x}_t, z_t, \hat{\mathbf{M}}_t) = \frac{\alpha}{2} + \frac{1 - \alpha}{4} \times \frac{\Phi_t(|\mathbf{x}_t - \mathbf{x}|) - \Phi_t(0)}{\Phi_t(d_{\max}) - \Phi_t(0)}$$

$$+ \frac{1 - \alpha}{4} \max_{(\hat{r}_l, \hat{\theta}_l) \in \hat{\mathbf{M}}_t} \left\{ \mathcal{C}(\mathbf{x}, \mathbf{x}_t, \hat{r}_l, \hat{\theta}_l) \times \right.$$

$$\left. \frac{\Gamma_{t,\hat{r}_l,\hat{\theta}_l}\left((x - x_t)\cos\hat{\theta}_l + (y - y_t)\sin\hat{\theta}_l\right) - \Gamma_{t,\hat{r}_l,\hat{\theta}_l}(0)}{\Phi_t(d_{\max}) - \Phi_t(0)} \right\}.$$

The first term of the sum accounts for echo mis-detection. The second one updates on-plate points with the detected echo up to a certain precision. The last term recovers areas outside the plate based on the estimated feature-based map which provides DoA estimates.

E. Inverse model estimation in the line space

As the mask $\hat{Q}_t$ is determined independently of the grid $\hat{O}_t$ with another binary filter, it is necessary to ensure sufficient consistency between the two grids so that the filtered lines are consistent with the estimated on-plate area. We propose an inverse model in the line space which maintains exact agreement in range and approximate consistency in angle from the former inverse model:

$$p(Q(r, \theta)|\mathbf{x}_t, z_t, \hat{\mathbf{M}}_t) = \frac{\alpha}{2} + \frac{1 - \alpha}{4} \times \frac{\Phi_t(d_t(r, \theta)) - \Phi_t(0)}{\Phi_t(d_{\max}) - \Phi_t(0)}$$

$$+ \frac{1 - \alpha}{4} \max_{(\hat{r}_l, \hat{\theta}_l) \in \hat{\mathbf{M}}_t} \left\{ \mathcal{C}'(\theta, \hat{\theta}_l) \times \right.$$

$$\left. \frac{\Gamma_{t,\hat{r}_l,\hat{\theta}_l}\left(|x_t \cdot \cos\hat{\theta}_l + y_t \cdot \sin\hat{\theta}_l - \hat{r}_l|\right) - \Gamma_{t,\hat{r}_l,\hat{\theta}_l}(0)}{\Phi_t(d_{\max}) - \Phi_t(0)} \right\}$$

where $\mathcal{C}'(\theta, \hat{\theta}_l) = \exp\{-\mu|\theta - \hat{\theta}_l|\}$. The exact consistency in range is indeed maintained as any line in the (r, θ) space is uniquely mapped to the orthogonal projection of the robot position on the line at each measurement step. Such an approach is convenient as the overall algorithm is computationally efficient and can run in real-time. Finally, we decide to filter out, on the beamforming maps, only the lines whose nonexistence is certain enough. Thus, the features $\hat{\mathbf{M}}_t$ are retrieved from $\hat{\mathcal{L}}_t(r, \theta) = \mathbf{1}_{\hat{Q}_t(r,\theta)>\tau} \cdot \mathcal{L}_t(r, \theta)$ where τ is chosen below 0.5.

IV. EXPERIMENTS AND RESULTS

We assess the performance of our approach in different scenarios. Experimental acoustic measurements are acquired, in the first one, by moving the transducers manually on an aluminum plate of dimensions 600x450x6mm. In the second scenario, the data are obtained in simulation for plates of varying sizes and sensor trajectories. In the last scenario, the measurements are acquired on a larger steel plate of 1700x1000x6mm with a magnetic crawler, manually driven with a joystick. To acquire the experimental data, we use two-tone bursts of a sinusoidal wave at 100kHz with an amplitude of 100V peak to peak to excite the wave in the plate material. Moreover, the incident signal is smoothly removed from the measurements as it does not correspond to a reflection on an edge. For all the trials, the parameters of the filter are: $\alpha = 0.7$, $\sigma = 1$cm, $b = 2$cm, $\gamma = 3$, $\mu = 2$ and $\tau = 0.2$. The
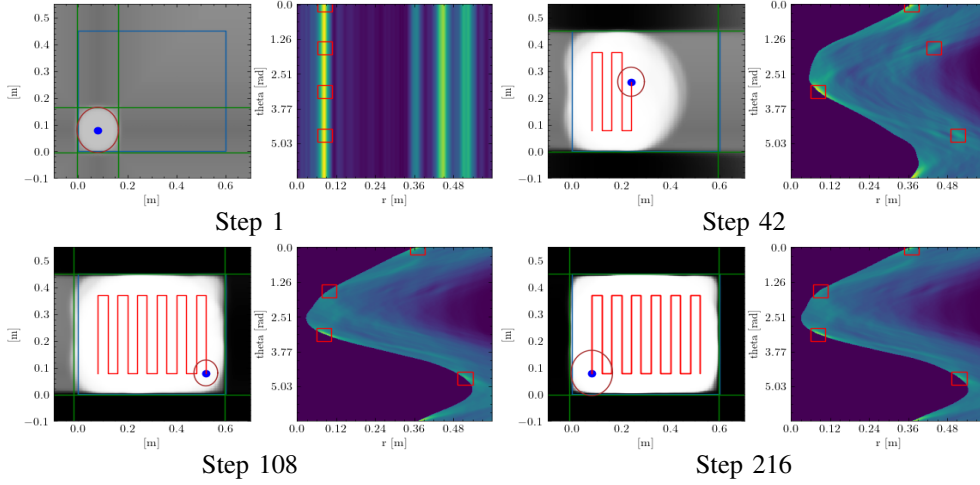
Fig. 2: Mapping results achieved on the aluminum plate during Steps 1, 42, 108 and 216. Each sub-figure depicts, on the left, the sensor trajectory along with the detected range to the closest edge represented by the circles, and on the right, the filtered beamforming maps during the same step, where the red rectangles indicate the retrieved edge estimates.

values of σ and b are consistent with the acoustic wavelength, approximately 2cm in our setups. The parameter α is set with a high value to limit the effect of one measurement update and increase the algorithm's robustness w.r.t. echo misdetection. The detection of the range to the closest edge is achieved with a standard peak detector applied to the correlation signals. The resulting performance is compared with that of a more standard mapping strategy [18] (that will serve as a baseline for comparison), where all the points within a given range are directly marked as inside the plate. The corresponding lines on the beamforming map are filtered out.

A. Evaluation with experimental measurements acquired manually and with simulated measurements

An emitter/receiver pair of transducers is placed by hand on the vertices of a 9×12 regular grid whose positions are carefully recorded on the aluminum plate. In total, 108 measurements were collected. We simulate a lawn-mower trajectory by using the theoretic displacement between measurement positions as flawless odometry. Fig. 2 shows the qualitative mapping results obtained with our approach at different steps of the scenario. The range to the closest edge is retrieved during the first step, but its orientation is ambiguous, resulting in a squared plate estimate. During Step 42, an essential portion of the plate has been correctly identified as "on the plate". Besides, the top and bottom sides of the plate have been marked as "outside the plate" based on the edge estimates retrieved from the filtered beamforming map. Nevertheless, the left edge has not been recovered because of interference that caused a line further away to be selected, as it cannot be filtered with our approach. During Step 108, all the edges are correctly retrieved from the filtered beamforming map. However, the area outside the plate on the left side has not yet been recovered because the edge estimation was incorrect when the mobile unit was close to it. This is achieved after simulating backwards the same trajectory, where the mapping is entirely achieved, as shown in Step 216. Ultimately, despite an average error of
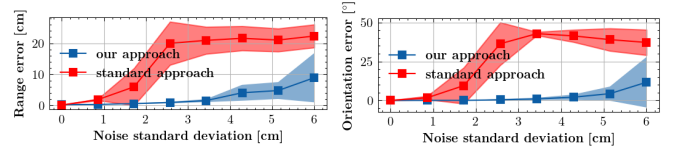

Fig. 3: Final mapping errors w.r.t. the noise level on the echo detection assessed over 10 repetitions of the lawnmower trajectory. The errors are determined both for our approach and for the baseline one. The left plot shows the range errors, while the orientation errors are shown on the right plot. The solid lines represent the average values, while the upper and lower bounds of the colored areas are situated respectively above and below one standard deviation to the mean values.

4.3cm on range detection, the mean estimation errors on the line parameters are 0.5cm for the ranges r_l, and are inferior to one degree for the orientations θ_l, $l = 1...4$. Furthermore, the two map representations can be considered coherent with each other, as only 7% of the plate points have been incorrectly identified as outside of it.

Hence, the results demonstrate the efficiency of our approach for mapping a plate structure with combined representations, where the grid can account for plate edges that are recovered at any time of the mapping process. However, the detected edges often lie at the limit of the

Plate size [mm]	Model	Range error [cm]	Angle error [degree]
600×450×6	Baseline	19.38 ± 4.83	33.46 ± 10.10
	Ours	$\mathbf{0.17 \pm 0.09}$	$\mathbf{0.44 \pm 0.37}$
1000×600×6	Baseline	31.73 ± 14.72	13.62 ± 15.10
	Ours	$\mathbf{0.12 \pm 0.11}$	$\mathbf{0.37 \pm 0.25}$
2000×1000×6	Baseline	69.62 ± 17.90	0.58 ± 0.89
	Ours	$\mathbf{1.59 \pm 3.59}$	$\mathbf{0.32 \pm 0.2}$

TABLE I: Average estimation errors and standard deviations on the lines parameters obtained in simulation, using our approach (in **bold**) and the baseline method.
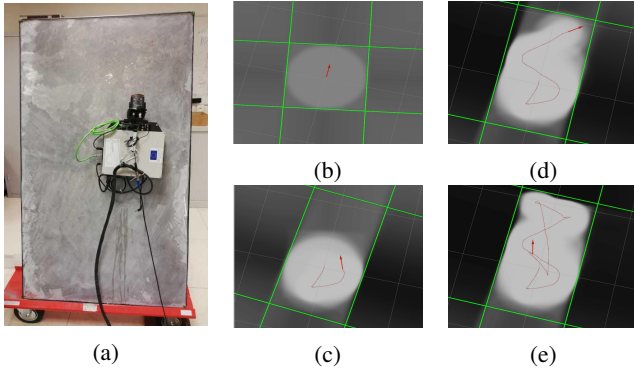
Fig. 4: Combined feature-based and grid-based mapping with a robotic platform relying on UGWs. (a) shows the experimental setup. (b), (c), (d) and (e) present the mapping results at different steps along the robot transect. The robot pose (red arrow) and trajectory (red line) are also represented.

filtered area. To assess the robustness of our approach, we evaluate the final average mapping errors over 10 repetitions of the lawnmower trajectory for varying noise levels on the echo detection. This is achieved by adding Gaussian noise to the ground truth range, determined based on the known acquisition positions. We do the same experience by using the baseline approach. Fig. 3 shows the results. It can be noticed that, with our approach, a range estimation error close to 1 cm and an orientation error of a few degrees at most are maintained for noise levels comparable to the wavelength. This is not the case with the baseline approach, where the estimation errors increase rapidly with the noise level, which illustrates its lack of robustness to map the inside of the plate with error-prone measurements.

To demonstrate that our method can generalize to various setups, we run it in simulation using data from three plates of different dimensions and a noise level of 5cm on echo detection. For comparison, we also repeat the process with the baseline approach. We provide the resulting average errors and standard deviations assessed over 50 repetitions of random paths (with a constant velocity) in Table I. It can be observed that, for the three scenarios, our approach achieves a higher precision than the baseline approach.

Overall, the results demonstrate the effectiveness of our method for mapping a plate while filtering beamforming maps to reduce the effect of interference (without completely alleviating it), even in the presence of echo detection errors.

B. Evaluation with a magnetic crawler

We evaluate our approach with a real robotic system and a large plate to demonstrate its viability for a practical robotic inspection task. In our experimental setup shown in Fig. 4a, the robot is equipped with an onboard accelerometer to provide accurate heading measurements and with a single transducer for both acoustic emission and reception. This setup requires using an electric circuit (whose implementation is not detailed here) for protecting the acquisition device during the emission at the cost of additional measurement perturbations. Also, a pump is activated to continuously bring water through

the tether at the interface between the sensor and the plate for sufficient coupling. During the acquisition, the robot is driven along a trajectory on the plate positioned nearly vertically, and the acquisition of one measurement is triggered each time the sensor has traveled 5 cm. For simplicity, we test our approach by assuming flawless odometry data, even though it is imperfect, and there may be slight errors in the kinematic model. However, the mapping procedure is expected to integrate seamlessly within a SLAM framework as in [1]. Figures 4b, 4c, 4d and 4e show the qualitative mapping results obtained with our approach at different steps of the robot transect. It can be observed that, at the early stage, the size of the plate is almost recovered as the estimated dimensions are $1798 \times 1012 mm$ during step (c), and the estimated orientation w.r.t. the robot is consistent with the reality (the full demonstration is available on the attached video). Besides, the inside and outside of the plate are correctly recovered, except for the regions near the corners, incorrectly marked as outside the plate. This slight inconsistency might be caused by the slight odometry errors and the increased complexity of the acoustic signals. Overall, these results demonstrate the applicability of our approach with a real robotic system. It may be useful for mapping a large structure made of several plates, as plate boundary detection is made robust, or by an active-sensing strategy for an optimal and autonomous mapping.

One of the limitations of our approach is that the parameters may be tuned carefully. Otherwise, proper lines may eventually be filtered on the beamforming map. In that situation, it is preferable to increase the noise parameters so that more measurements would be necessary before a line is filtered out. Also, our approach is evaluated on an isolated plate in a laboratory environment, while real metal structures present complex structural features such as welds or stiffeners. The constraint of rectangular shapes is not a limitation for mapping storage tanks or ship hulls, as they are almost entirely made of rectangular panels. However, extensions of our approach may be investigated to work with more general structures. It is expected it would only require an extension of the optimization method presented in [1] to retrieve the edges from the beamforming maps. At the same time, the design of the Bayesian framework could be left unchanged.

V. CONCLUSION

This work presents a novel framework for mapping structures made of metal plates with combined representations and UGW measurements. It is based on inverse sensor models estimated online to build a grid representation, along with a binary filter applied to the beamforming maps to mitigate interference. The results demonstrate its effectiveness and robustness to echo misdetection, while its practical use is highlighted by using a real robotic platform. The approach shall be evaluated in more realistic scenarios within a SLAM framework, and the relaxation of the constraint of rectangular shapes shall be considered. Also, active-sensing strategies relying on such representations shall be investigated for optimal and autonomous reconstruction, while the mapping of defects must be integrated for inspection purposes.

REFERENCES

[1] O. L. Ouabi, P. Pomarede, M. Geist, N. F. Declercq, and C. Pradalier, "A FastSLAM Approach Integrating Beamforming Maps for Ultrasound-Based Robotic Inspection of Metal Structures," *IEEE Robotics and Automation Letters*, vol. 6, no. 2, pp. 2908–2913, 2021.

[2] "Bugwright2, autonomous robotic inspection and maintenance on ship hulls and storage tanks. Grant agreement of the innovative action. Horizon 20200 - Work programme. Information and communication technologies (ICT-09-2019-2020)," 2020.

[3] Z. Su and L. Ye, *Identification of damage using Lamb waves: from fundamentals to applications*. Springer Science & Business Media, 2009, vol. 48.

[4] Z. Liu and H. Chen, "Application and Challenges of Signal Processing Techniques for Lamb Waves Structural Integrity Evaluation: Part A-Lamb Waves Signals Emitting and Optimization Techniques," *Structural Health Monitoring from Sensing to Processing*, vol. 32, no. July, pp. 137–144, 2018.

[5] S. Thrun, W. Burgard, and D. Fox, *Probabilistic Robotics.*, ser. Intelligent robotics and autonomous agents. MIT Press, 2005.

[6] B. D. Van Veen and K. M. Buckley, "Beamforming: a versatile approach to spatial filtering," *IEEE ASSP Magazine*, 1988.

[7] "Roboplanet, robots for human and industrial and safety." [Online]. Available: http://www.roboplanet.fr/en/

[8] J. S. Hall, P. McKeon, L. Satyanarayan, J. E. Michaels, N. F. Declercq, and Y. H. Berthelot, "Minimum variance guided wave imaging in a quasi-isotropic composite plate," *Smart Materials and Structures*, vol. 20, no. 2, 2011.

[9] N. Quaegebeur, P. Masson, D. Langlois-Demers, and P. Micheau, "Dispersion-based imaging for structural health monitoring using sparse and compact arrays," *Smart Materials and Structures*, vol. 20, no. 2, 2011.

[10] J. S. Hall and J. E. Michaels, "Multipath ultrasonic guided wave imaging in complex structures," *Structural Health Monitoring*, vol. 14, no. 4, pp. 345–358, 2015.

[11] E. Hong and C. Schaal, "Reverse engineering stiffened plates using guided wave-based nondestructive testing methods," in *Health Monitoring of Structural and Biological Systems XII*, vol. 10600. International Society for Optics and Photonics, 2018, p. 106000E.

[12] C. Schaal, M. Brown, and K. Schulz, "Experimental investigation of lamb wave-based edge detection methods," in *Health Monitoring of Structural and Biological Systems XIII*, vol. 10972. International Society for Optics and Photonics, 2019, p. 1097223.

[13] O.-L. Ouabi, P. Pomarede, M. Geist, N. F. Declercq, and C. Pradalier, "Monte-Carlo Localization on Metal Plates Based on Ultrasonic Guided Waves," in *The 17th International Symposium on Experimental Robotics*, 2021, pp. 345–353.

[14] C. Pradalier, O. L. Ouabi, P. Pomarede, and J. Steckel, "On-plate localization and mapping for an inspection robot using ultrasonic guided waves: A proof of concept," *IEEE International Conference on Intelligent Robots and Systems*, pp. 5045–5050, 2020.

[15] M. Montemerlo, S. Thrun, D. Koller, and B. Wegbreit, "Fastslam: A factored solution to the simultaneous localization and mapping problem," *Aaai/iaai*, 2002.

[16] H. H. González-Baños and J.-C. Latombe, "Navigation strategies for exploring indoor environments," *The International Journal of Robotics Research*, vol. 21, no. 10-11, pp. 829–848, 2002.

[17] B. Yamauchi, "A frontier-based exploration for autonomous exploration," *IEEE International Symposium on Computational Intelligence in Robotics and Automation, Monterey, CA*, pp. 146–151, 1997.

[18] A. Miranda, J. V. Hook, and C. Schaal, "Lamb wave-based mapping of plate structures via frontier exploration," *Ultrasonics*, vol. 110, no. September 2020, p. 106282, 2021. [Online]. Available: https://doi.org/10.1016/j.ultras.2020.106282

[19] K. M. Wurm, C. Stachniss, and G. Grisetti, "Bridging the gap between feature- and grid-based SLAM," *Robotics and Autonomous Systems*, vol. 58, no. 2, pp. 140–148, 2010. [Online]. Available: http://dx.doi.org/10.1016/j.robot.2009.09.009

[20] A. K. Pandey, K. M. Krishna, and M. Nath, "Feature based occupancy grid maps for sonar based safe-mapping," *IJCAI International Joint Conference on Artificial Intelligence*, pp. 2172–2177, 2007.

[21] F. Andert and L. Goormann, "Combined grid and feature-based occupancy map building in large outdoor environments," *IEEE International Conference on Intelligent Robots and Systems*, pp. 2065–2070, 2007.

[22] M. Kreković, I. Dokmanić, and M. Vetterli, "Echoslam: Simultaneous localization and mapping with acoustic echoes," in *IEEE International Conference on Acoustics, Speech and Signal Processing*, 2016.

[23] F. Peng, T. Wang, and B. Chen, "Room shape reconstruction with a single mobile acoustic sensor," in *2015 IEEE Global Conference on Signal and Information Processing (GlobalSIP)*. IEEE, 2015.

[24] S. Thrun, "Learning occupancy grids with forward models," *IEEE International Conference on Intelligent Robots and Systems*, vol. 3, pp. 1676–1681, 2001.